Electronic and Structural Properties of the (10$\bar{1}$0) and (11$\bar{2}$0) ZnO Surfaces

N. L. Marana,[‡] V. M. Longo,[§] E. Longo,[§] J. B. L. Martins,*[,||] and J. R. Sambrano*[,‡]

Grupo de Modelagem e Simulação Molecular, DM, Universidade Estadual Paulista, P.O. Box 473, 17033-360 Bauru, SP. Brazil, LIEC, DQ, UFSCar, P.O. Box 676, 13565-905, São Carlos, SP. Brazil, and Instituto de Química, Universidade de Brasília, CP 4478, Brasília, DF, 70904-970, Brazil

Received: February 27, 2008; Revised Manuscript Received: April 30, 2008

The structural and electronic properties of ZnO (10$\bar{1}$0) and (11$\bar{2}$0) surfaces were investigated by means of density functional theory applied to periodic calculations at B3LYP level. The stability and relaxation effects for both surfaces were analyzed. The electronic and energy band properties were discussed on the basis of band structure as well as density of states. There is a significant relaxation in the (10$\bar{1}$0) as compared to the (11$\bar{2}$0) terminated surfaces. The calculated direct gap is 3.09, 2.85, and 3.09 eV for bulk, (10$\bar{1}$0), and (11$\bar{2}$0) surfaces, respectively. The band structures for both surfaces are very similar.

1. Introduction

Zinc oxide is widely used in technological applications because of its unique electronic and electro-optical properties. Its structural and electronic properties are also of interest because of its importance in catalysis, for example, methanol synthesis. Recently, the successful growth of nanomaterials has increased its potential applications.[1–5]

ZnO crystallizes in the wurtzite structure (B4) at room temperature. The wurtzite morphology is characterized by four low-index surfaces, that is, the nonpolar prism (10$\bar{1}$0) and (11$\bar{2}$0) surfaces, along with the polar or basal (0001)-Zn and (000$\bar{1}$)-O surfaces.[6–10] The ZnO wurtzite structure consists of hexagonal Zn and O planes stacked alternately, along the *c*-axis with each O^{2-} ion surrounded by a tetrahedron of Zn^{2+} ions and vice versa.

ZnO surfaces have attracted substantial attention in recent years because of the wide band gap semiconductor, where it finds a wide variety of applications such as catalysis and most recently nanomaterials.[11] The structure and morphology of ZnO are decisive for the atomic-scale growth of nanomaterials. ZnO nanoparticles and nanorods/wires have been intensively studied for promising applications as gas sensors, photodetectors, and optoelectronic devices.[12] However, before these interesting applications of ZnO can be addressed, a thorough understanding of the underlying clean ZnO surfaces is necessary. ZnO is also a particularly attractive material for luminescent nanoparticle applications because of its wide band gap and stability to intense ultraviolet emission.[13] Considering the wide usage of the ZnO surface as a catalyst, there is insufficient theoretical data on its nonpolar low index surfaces.[6–10,14–29] Various experimental techniques and theoretical methods have been used to study the different surfaces of ZnO. The two polar ZnO surfaces are the most intriguing ones, where the Zn and O sides of a crystal have different physical and chemical properties.[8]

The mixed covalent and ionic aspects, in the chemical bonding of ZnO, play an important role in the surface catalytic activity. On the other hand, ZnO shows great similarities with ionic insulators such as MgO.[30] From a physical and chemical point of view, the electronic properties of the ZnO surfaces are very important in chemical gas sensors and catalysts. Furthermore, ZnO has a great contribution to the nanotechnology, and the role played by the polar surfaces is especially important. As a result, various polar-surface-dominated nanostructures have been found for wurtzite ZnO.[31]

ZnO (0001) and (000$\bar{1}$) polar surfaces are quite stable without faceting or exhibiting massive surface reconstructions. Electrostatic consideration and electronic structure calculation suggest that a rearrangement of charges on both outmost layers of a ZnO crystal may cancel the polarity.[31,32]

(10$\bar{1}$0) surfaces perpendicular to the *c*-axis are composed by Zn−O dimers with neutral charge, forming the nonpolar surfaces. The dangling bonds on such surfaces make the system unstable.[33] It was considered that the Zn−O surface dimers on nonpolar (10$\bar{1}$0) surface are energetically favorable after a slight tilting and an inward displacement into the volume.[15]

In general, the nonpolar surfaces of many semiconductors undergo symmetry conserving relaxations from the bulk geometry to one of the lower free energy (ground state, zero temperature). The nonpolar (10$\bar{1}$0) surface of the wurtzite structure is believed to undergo a relaxation, where bonds between adjacent anions and cations in the outermost layer shorten. These surface dimers tilt in such a way that the anions are in the outermost layer. In order to understand these electronic properties and structure−reactivity relationship, an accurate knowledge of the clean surfaces is necessary. In spite of extensive theoretical calculations of (10$\bar{1}$0) surface, the electronic structure and relative stability of relaxed (11$\bar{2}$0) surface have been the subject of a few studies only.

In this paper, we report periodic first-principle calculations based on density functional theory (DFT) in order to investigate the structural and electronic properties of hexagonal wurtzite ZnO in the bulk and the (10$\bar{1}$0) and (11$\bar{2}$0) nonpolar surface structures. The results are discussed in terms of density of states (DOS), band structures, and charge distributions and compared with reported quantum mechanical calculations, as well as available experimental data.

2. Computational Method and Periodic Model System

Zinc oxide crystallizes in rocksalt (NaCl), zincblende, and hexagonal wurtzite structures.[34,35] The thermodynamically stable

† Part of the special section for the "Symposium on Energetics and Dynamics of Molecules, Solids and Surfaces".

* Corresponding authors. E-mail: sambrano@fc.unesp.br and lopes@unb.br.
‡ Universidade Estadual Paulista.
§ LIEC.
|| Universidade de Brasília.

10.1021/jp801718x CCC: $40.75
Published on Web 07/02/2008

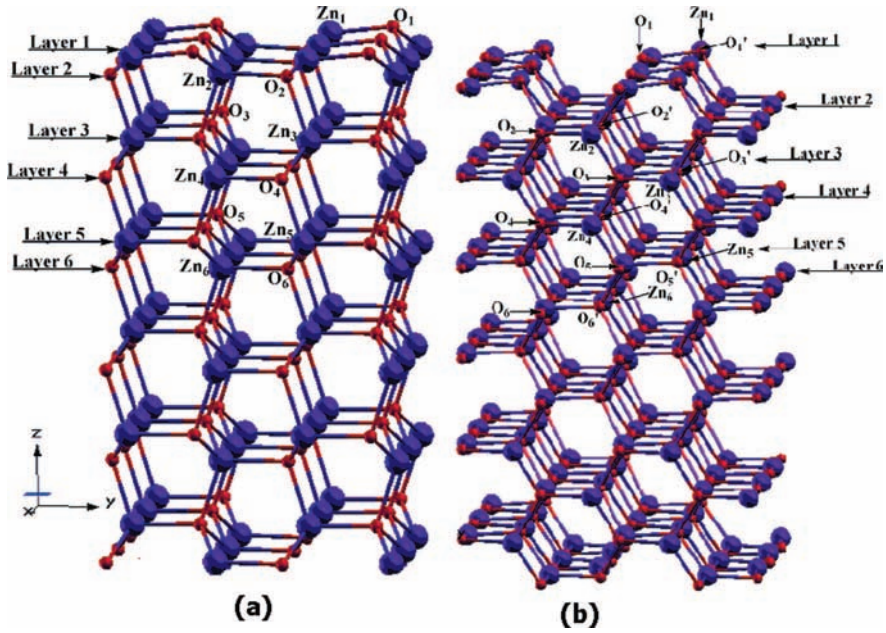

Figure 1. Surface slab models of (a) (10$\bar{1}$0) and (b) (11$\bar{2}$0) surfaces.

TABLE 1: Cell Parameters (Angstrom), Internal Parameter *u*, *c/a* Distortion (Angstrom), Volume (Å^3), and Relative Deviations from Experimental Value in Parentheses (Given in Percents)

	a	*c*	*u*	*c/a*	V_0
B3LYP [this work]	3.259 (0.28)	5.205 (−0.04)	0.382 (−0.08)	1.697 (5.86)	47.87 (0.44)
B3LYP[51]	3.253 (0.09)	5.207 (0)	0.385 (0)	1.601 (−0.12)	47.97 (0.65)
HF[34]	3.290 (1.23)	5.241 (0.65)	0.385 (0)	1.593 (−0.62)	49.14 (−3.01)
HF[51]	3.290 (1.23)	5.200 (−0.13)	0.385 (0)	1.580 (−1.43)	47.78 (0.25)
Exp[49]	3.250	5.207	0.385	1.603	47.66

phase wurtzite (under normal conditions) was studied. It belongs to the space group $P6_3mc$, and each anion is surrounded by four cations at the corners of a tetrahedron.

The periodic DFT calculations with the B3LYP hybrid functional[36,37] were performed by using the CRYSTAL03 computer code.[38] The B3LYP functional is known to simulate the energetic, geometric, and electronic properties of materials with significantly greater accuracy.[39] This functional has been successfully employed for studies of the electronic and structural properties of diverse compounds.[40–42]

The atomic centers have been described by all-electron basis set 6-31G* for Zn[43] and O[38,44] atoms.

As a first step, we have carried out the optimization of the exponents for the outermost sp and d shells in order to minimize the total energy of the structure at experimental parameters. The optimized external exponents are $\alpha_{sp}(Zn) = 0.143264$, $\alpha_d(Zn) = 0.730294$, and $\alpha_{sp}(O) = 0.274200$. Powel's algorithm[45] method has been used to perform all optimization procedure.

From this optimized parameters, a new optimization procedure of the lattice parameters, *a*, *c*, and *u* has been performed. In the next step, two surfaces structures (10$\bar{1}$0) and (11$\bar{2}$0) have been modeled, by taking into account the mirror symmetry with respect to the central layers, by unreconstructed (truncated bulk) slab models using the calculated equilibrium geometry. These slabs are finite in the *z*-direction but periodic in the *x*- and *y*-directions, and the periodically repeating unit cells representing both slabs are depicted in Figure 1. Full relaxation of these surfaces has been performed.

The band structures were obtained for 80 $\vec{k}$ points along the appropriate high-symmetry paths of the adequate Brillouin zone. Diagrams of the DOS were calculated for analysis of the corresponding electronic structure. The XcrysDen program[46] has been used for the design of band structure and DOS diagram.

3. Results and Discussion

3.1. Structural and Electronic Bulk Properties. The theoretical lattice parameters and other theoretical and experimental data are displayed in Table 1. Our results are only 0.28% larger than experimental data for the *a* parameter and −0.04 and −0.08% lower for the *c* parameter and the internal parameter *u*, respectively. Goano et al.[47] present a detailed review of lattice constants and internal parameter of wurtzite ZnO. The most recent lattice parameters were taken from Decremps et al.[48] by using extended X-ray absorption fine structure, and the values are $a = 3.258$ and $c = 5.220$Å. Our results are in good agreement with the other theoretical and experimental data.[34,35,47,49–51] The Zn−O distance is 1.979 Å, whereas the overlap is 132 mlel, and the Mulliken charges are Zn = 1.071au and O = −1.07au.

Figure 2a represents the band structure of the bulk ZnO. Table 2 shows the calculated Fermi energies and optical gaps. The top of the valence band (VB), coincident with the origin, is located at the Γ point. The band gap is direct, 3.09 eV, in accordance to the experimental optically measured gap[35,52] and other theoretical works.[21,51]

An analysis of the DOS for bulk model, shown in Figure 3a, indicates that the VB consists mainly of 2p levels of O atoms with a minor contribution of 4s4p, and the intense peak is due to 3d orbitals of Zn atoms. The main contribution of conduction band (CB) comes from 4s4p levels of Zn atoms.

3.2. Surface Models. The (10$\bar{1}$0) and (11$\bar{2}$0) surfaces has been the object of previous theoretical works.[10,21,22,24,25,51,53] The

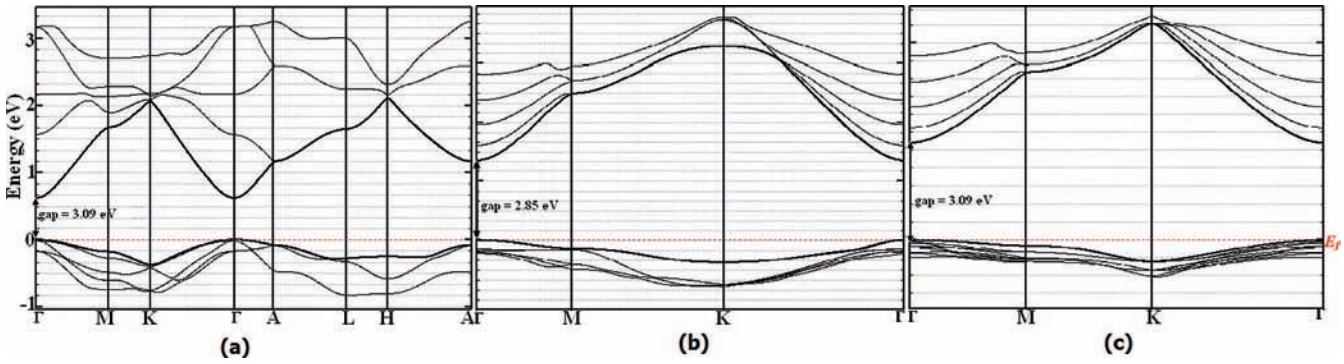

Figure 2. Band structure for the (a) bulk, (b) $(10\bar{1}0)$, and (c) $(11\bar{2}0)$ surface models.

TABLE 2: Calculated Fermi Energy (E_f) and Band Gap (eV) for the bulk, $(10\bar{1}0)$, and $(11\bar{2}0)$ surfaces

	bulk	$(10\bar{1}0)$	$(11\bar{2}0)$
E_f	−4.95	−5.88	−6.23
Γ−Γ	3.09	2.85	3.09
K−K	7.54	5.56	7.54
M−M	5.51	5.65	5.51
Γ−M	5.33	5.25	5.33
K−Γ	6.86	4.08	6.86
K−M	7.04	7.25	7.04
gap exp.	3.40[35]	3.30[58]	

$(10\bar{1}0)$ has been the focus of many theoretical end experimental researches and is the easiest surface to treat theoretically. Both surfaces are formed by atomic planes of Zn−O dimers (See Figure 1).

The first problem to build a surface computational model is selecting the number of the layers in the slab. For this purpose, we have calculated the surface energy, E_{surf}, and Table 3 shows the results of these optimized energies calculated by using 8−18 layers. To our knowledge, this is the first use of 18 layers for the study of ZnO nonpolar surfaces.

The E_{surf} for $(10\bar{1}0)$ and $(11\bar{2}0)$ surfaces are 1.3 and 1.4 J/m^2, respectively from 12 to 18 layers. This energy has converged to its infinite thickness. Nevertheless, in order to confirm the convergence of slab thickness, we calculated the Mulliken charge distributions (Table 4) at the bulk terminated geometry for the different models. The choice of a Mulliken partition is arbitrary, because there is no unique method of performing the partition of the charge density. However, the choice of a given scheme is still extremely useful in comparing the tendencies in the results of calculations performed by using similar models. The analyses yields convergence for 12−18 layers for both surfaces. Consequently, 12 layers may be sufficient to describe the surface geometry and appropriate system for relaxation model studies and is used throughout the text for the properties analysis.

The difference found for surface energy is 0.1 J/m^2, suggesting that the $(10\bar{1}0)$ surface is more stable than the $(11\bar{2}0)$ surface. This result is in agreement with other theoretical works. In particular, Meyer et al.[11] carried out a theoretical investigation of the nonpolar $(10\bar{1}0)$ and $(11\bar{2}0)$ surfaces. These authors discuss the stability of the surfaces in terms of cleavage energy and show that the $(10\bar{1}0)$ surface is more stable that the $(11\bar{2}0)$ surface with a slight difference, 0.2 J/m^2. However, this work[11] carried out a partial optimization of nonpolar surfaces. It is important to note that the calculated cleavage and surface energies depend on the theory level, basis set, and Hamiltonian (functional) employed. The large number of layers used and also the difference between full relaxation and the relaxation of the first two surface layers may be the key for our smaller difference of E_{surf} between $(10\bar{1}0)$ and $(11\bar{2}0)$ surfaces. Other theoretical works also maintain the inner atoms to the bulk periodicity,[21,23] whereas our relaxations with full optimization results indicate that the inner layers are slightly modified. In order to corroborate this trend, we have performed B3PW hybrid density functional calculations (by using PWGGA for the nonlocal correlation part), and the same order for the surface energy was obtained. However, this difference found for the surface energy by comparing with other theoretical works indicates that new approaches need to be used in order to clarify our results.

Table 5 shows the atomic displacements for both surfaces. The effect of optimization has been analyzed for these surfaces by relaxing all atomic positions in *x*-, *y*-, and *z*-directions. The positive displacements in the *z*-direction indicate relaxations toward the vacuum, and the magnitudes are measured with respect to the bulk truncated atomic positions. When Δx is close to zero, the value is not reported. The calculated tilt angle (Figure 3 of ref 11) for the $(10\bar{1}0)$ surface is 6.55°, whereas it is 7.63° for the $(11\bar{2}0)$ surface. These values are smaller than the tilt angle of 10.7° for the $(10\bar{1}0)$ surface found by using LDA.[11]

The $(10\bar{1}0)$ 12-layer surface indicates that the largest relaxations in *z*-direction are on the first and second layer for Zn atoms, which includes a displacement of second-layer O atoms of 0.042 Å. In the *y*-direction, the largest deviations occur for the first-layer Zn atom. The larger magnitude of Zn relaxation, compared to O atoms, leads to surface roughness at the first and second layers, in accordance to the experimental studies.[8,9]

The experimental and theoretical studies of $(10\bar{1}0)$ surface relaxation are controversial (Table 6). Duke et al.[15] concluded from low-energy electron diffraction (LEED) analysis that the top-layer Zn ion is displaced downward by 0.45 Å and the O is displaced by 0.05 Å. More recently, Jedrecy et al.,[6] by using grazing incidence X-ray diffraction (GIXD), found a top-layer Zn atom displaced downward by only −0.06 Å. The O position shows some uncertainty in the experimental values.[6,31] There is some convergence among the several theoretical results for the O displacement, which shows the O atom above the Zn atom.[10,11,17–19,21,23,24,54] Our theoretical full relaxation results for Zn and O atoms are in agreement with the atomistic potential models.[23] There is no significant relaxation below the second layer, which is in accordance with the high-resolution transmission electron microscopy (HRTEM) results.[31]

The $(11\bar{2}0)$ surface has a small relaxation in *z*-direction with the same trend of O above the Zn atom. There is a disagreement in the literature regarding the $(11\bar{2}0)$ relaxation. Wander and Harrison[22] found the $(11\bar{2}0)$ surface bulk terminated with only a small relaxation of the Zn atom of −0.03Å by using B3LYP

Figure 3. Total and projected DOS (arbitrary units) for the (a) bulk, (b) (10$\bar{1}$0), and (c) (11$\bar{2}$0) surfaces.

TABLE 3: Surface Energy (J/m^2) for (10$\bar{1}$0) and (11$\bar{2}$0) surfaces

	(10$\bar{1}$0)	(11$\bar{2}$0)
8	1.4	1.4
10	1.4	1.4
12	1.3	1.4
14	1.3	1.4
16	1.3	1.4
18	1.3	1.4

and a small slab of seven layers without a full relaxation. The tight binding model of Wang and Duke[55] study of (11$\bar{2}$0) surface predicted the same relaxation behavior found for the (10$\bar{1}$0) surface; they found a strong Zn displacement of −0.54Å. Atomistic approach with the potential parameters of Nyberg et al.[19] led to a displacement downward by −0.15 Å. Dulub et al.[8] studied the polar and nonpolar ZnO surfaces by using scanning tunneling microscopy and concluded that the nonpolar (11$\bar{2}$0) surface of ZnO is the roughest of all the investigated surfaces.

The calculated value for the Zn−O dimer distance at the first layers is slightly lower than experimental data reported by Jadrecy et al.[6] and other theoretical works.[21,50] When comparing the calculated bond distance in relation to the bulk value of 1.979 Å, the Zn−O first layer presents a bond shortening. The overlap population serves as a version of bond order for solids

TABLE 4: Distances (Angstrom) of Zn−O Bonds of Uppermost Six Layers, Mulliken Charge Distribution (*Q* |e|), and Overlap Population (m|e| in Parentheses)

$(10\bar{1}0)$	*Q* (Zn)	*Q* (O)	$(11\bar{2}0)$	*Q* (Zn)	*Q* (O)
		1st layer			
Zn_1-O_1 1.861 (192)	1.00	−0.98	Zn_1-O_1 1.877 (175) Zn_1-O_1' 1.893 (169)	1.00	−0.99
		2nd layer			
Zn_2-O_2 1.982 (109) Zn_1-O_2 1.924 (135)	1.02	−1.05	Zn_2-O_2 1.986 (125) Zn_2-O_2' 1.974 (126) Zn_1-O_2 1.954 (127)	1.04	−1.06
		3rd layer			
Zn_3-O_3 1.978 (140) Zn_2-O_3 2.057 (106)	1.07	−1.06	Zn_3-O_3 1.992 (133) Zn_3-O_3' 1.989 (133) Zn_2-O_3 2.016 (122)	1.07	−1.07
		4th layer			
Zn_4-O_4 1.998 (125) Zn_3-O_4 1.970 (133)	1.06	−1.07	Zn_4-O_4 1.995 (130) Zn_4-O_4' 1.989 (131) Zn_3-O_4 1.982 (133)	1.07	−1.07
		5th layer			
Zn_5-O_5 1.993 (131) Zn_4-O_5 1.997 (129)	1.07	−1.07	Zn_5-O_5 1.992 (130) Zn_5-O_5' 1.988 (131) Zn_4-O_5 1.988 (132)	1.07	−1.07
		6th layer			
Zn_6-O_6 1.995 (129) Zn_5-O_6 1.983 (132)	1.07	−1.07	Zn_6-O_6 1.993 (130) Zn_6-O_6' 1.988 (132) Zn_5-O_6 1.988 (131)	1.07	−1.07

TABLE 5: Displacements of Zinc and Oxygen Atoms, Δ*x*, Δ*y*, and Δ*z* (Angstrom) of Uppermost Six Layers from their Ideal Lattice Positions

	$(10\bar{1}0)$		$(11\bar{2}0)$		
	Δ*y*	Δ*z*	Δ*x*	Δ*y*	Δ*z*
Zn_1	0.116	−0.210	0.085	−0.156	−0.093
O_1	−0.024	0.002	−0.041	0.010	0.064
Zn_2	−0.020	0.135	−0.017	−0.025	0.117
O_2	−0.028	0.042	−0.020	0.018	0.075
Zn_3	0.003	−0.001	−0.006	−0.007	0.050
O_3	−0.008	0.050	−0.002	0.018	0.071
Zn_4	−0.015	0.049	−0.007	0.000	0.049
O_4	−0.006	0.024	−0.001	0.012	0.042
Zn_5	−0.005	0.011	0.000	0.001	0.026
O_5	−0.001	0.026	0.004	0.010	0.029
Zn_6	−0.009	0.011	0.000	0.002	0.010
O_6	−0.002	0.001	0.005	0.010	0.008

TABLE 6: Experimental and Theoretical ΔZ Displacement of Zn and O Atoms of $(10\bar{1}0)$ Surface

	Zn_1	O_1	Zn_2	O_2
DFT (this work)	−0.210	0.002	0.135	0.042
LEED[15]	−0.450	−0.050	0	0.100
RHF[18]	−0.259	−0.184		
RHF+corr[18]	−0.246	−0.166		
DFT LDA[17]	−0.320	−0.200		
GULP/AIMP[19]	−0.220	−0.260	0.080	0.100
DFT LDA[54]	−0.500	−0.130	−0.090	−0.090
GIXD[6]	−0.060	−0.120		
B3LYP[21]	−0.312	−0.161		
SXRD[7]	∼0	∼0	∼0	∼0
Atomistic potentials[23]	−0.250	0.036	0.165	0.070
PW LDA[11]	−0.360	−0.040		
PW DFT[24]	−0.285	−0.041		
PW DFT[10]	−0.330	−0.050		
HRTEM[31]	−0.370	-	0.480	-

and is also used for the X-ray absorption near-edge structure peak assignments.[56] The value of overlap population is larger for the outermost layers, which indicates that the outermost layers are stable. It may be meaningful to associate shortening of a bond with an increase in the overlap population and also a greater Coulombic attraction.

Table 4 shows the Zn−O bond distances of the six uppermost layers, Mulliken charge distribution, and overlap population. From Table 4, the distance of Zn−O bonding in the same layer are very similar. The overlap population value of the first layer is 192 and 175 m|e| for the $(10\bar{1}0)$ and $(11\bar{2}0)$ surface, respectively. The overlap population of the inner layer (6th) is smaller than that of the first layer. This is probably due to a covalent character increase of Zn−O bonding for the $(11\bar{2}0)$ surface.

3.2.1. Surface Band Structure and DOS. Figure 2b,c represents the band structures for both relaxed surfaces. Table 2 gathers the calculated and experimental optical gaps and Fermi energies.

The top of the upper VB, coincident with the origin, and the bottom of the lowest CB for $(10\bar{1}0)$ and $(11\bar{2}0)$ surfaces (see Figure 2b,c) are located at the Γ point of the 2D Brillouin zone. The band gap for the $(10\bar{1}0)$ surface is reduced to 2.85 eV compared with the bulk value. On the other hand, the energy gap of the $(11\bar{2}0)$ surface is coincident with the calculated bulk band gap, 3.09 eV, because their optimized atomic relaxation are very small, and the geometry is similar to the bulk. The band structures are very close for both surfaces. To our knowledge, there is no reported gap value for the $(11\bar{2}0)$ surface.

We have calculated the DOS in order to understand the band structure. Figure 3 depicts the total and atom projected DOS for both surface structures. The analyses of the principal atomic orbital (AO) components of selected bands were performed with the ANBD option of the CRYSTAL03 code by using a threshold of 0.15 au for the important eigenvector coefficients.[57]

For the $(10\bar{1}0)$ surface, AO contributions show that the top of the VB bands is mainly derived by first- and second-layers Zn and first-layer O atoms. The $2p_x$ and $2p_z$ orbital of O atoms can be considered as bands of surface states. The upper zone of CB is mainly made from s and d orbitals of Zn surface atoms.

The top of VB for the $(11\bar{2}0)$ surface consists mainly of O and Zn atoms belonging to the first layer. The principal AO

component is made of 2p orbital of O surface atoms. Only the Zn atoms have significant contribution to the CB.

4. Conclusions

Computational studies, based on first-principle periodic calculations, can be important for elucidating the electronic and structural properties of materials. We have performed periodic B3LYP calculations of ZnO $(10\bar{1}0)$ and $(11\bar{2}0)$ in order to study the relaxation effects. The conclusions are summarized below.

1. The calculated structural and electronic bulk properties are in good agreement with other theoretical and experimental data.

2. The $(10\bar{1}0)$ and $(11\bar{2}0)$ 12-layer surface indicates that the largest relaxations in *z*-direction are on the first and second layer for Zn atoms.

3. The calculated value for the Zn−O dimer distance in relation to the bulk value of 1.979 Å the Zn−O first layer presents a bond shortening.

4. The band gap for $(10\bar{1}0)$ surface is reduced to 2.85 eV compared with the bulk value.

5. The energy gap of $(11\bar{2}0)$ surface is coincident with the calculated bulk band gap, 3.09 eV, because the optimized atomic relaxation is very small.

6. The top of VB for the $(11\bar{2}0)$ surface consists mainly of O and Zn atoms belonging to the first layer.

Acknowledgment. This work was supported by Brazilian Funding Agencies FAPESP, CAPES, CNPq, Finatec, and UnB.

References and Notes

(1) Orlandi, M. O.; Ramirez, A. J.; Leite, E. R.; Longo, E. *Cryst. Growth Des.* **2008**, *8*, 1067.
(2) Viswanatha, R.; Chakraborty, S.; Basu, S.; Sarma, D. D. *J. Phys. Chem. B* **2006**, *110*, 22310.
(3) Yan, C. L.; Xue, D. *J. Phys. Chem. B* **2006**, *110*, 25850.
(4) Silva, C. C.; Filho, F. P.; Sombra, A. S. B.; Rosa, I. L. V.; Leite, E. R.; Longo, E.; Varela, J. A. *J. Fluoresc.* **2008**, *18*, 253.
(5) Giraldi, T. R.; Escote, M. T.; Maciel, A. P.; Longo, E.; Leite, E. R.; Varela, J. A. *Thin Solid Films* **2006**, *515*, 2678.
(6) Jedrecy, N.; Gallini, S.; Sauvage-Simkin, M.; Pinchaux, R. *Surf. Sci.* **2000**, *460*, 136.
(7) Lindsay, R.; Thornton, G. *Top. Catal.* **2002**, *18*, 15.
(8) Dulub, O.; Boatner, L. A.; Diebold, U. *Surf. Sci.* **2002**, *519*, 201.
(9) Diebold, U.; Koplitz, L. V.; Dulub, O. *Appl. Surf. Sci.* **2004**, *237*, 336.
(10) Cooke, D. J.; Marmier, A.; Parker, S. C. *J. Phys. Chem. B* **2006**, *110*, 7985.
(11) Meyer, B.; Marx, D. *Phys. Rev. B* **2003**, *67*, 35403.
(12) Zhang, P.; Xu, F.; Navrotsky, A.; Lee, J. S.; Kim, S. T.; Liu, J. *Chem. Mater.* **2007**, *19*, 5687.
(13) Prades, J. D.; Cirera, A.; Morante, J. R.; Comet, A. *Thin Solid Films* **2007**, *515*, 8670.
(14) Duke, C. B.; Lubinsky, A. R.; Chang, S. C.; Lee, B. W.; Mark, P. *Phys. Rev. B* **1977**, *15*, 4865.
(15) Duke, C. B.; Meyer, R. J.; Paton, A.; Mark, P. *Phys. Rev. B* **1978**, *18*, 4225.
(16) Lafemina, J. P.; Duke, C. B. *J. Vac. Sci. Technol. A* **1991**, *9*, 1847.
(17) Schroer, P.; Kruger, P.; Pollmann, J. *Phys. Rev. B* **1994**, *49*, 17092.
(18) Jaffe, J. E.; Harrison, N. M.; Hess, A. C. *Phys. Rev. B* **1994**, *49*, 11153.
(19) Nyberg, M.; Nygren, M. A.; Pettersson, L. G. M.; Gay, D. H.; Rohl, A. L. *J. Phys. Chem.* **1996**, *100*, 9054.
(20) Parker, T. M.; Condon, N. G.; Lindsay, R.; Leibsle, F. M.; Thornton, G. *Surf. Sci.* **1998**, *415*, L1046.
(21) Wander, A.; Harrison, N. M. *Surf. Sci.* **2000**, *457*, L342.
(22) Wander, A.; Harrison, N. M. *Surf. Sci.* **2000**, *468*, L851.
(23) Whitmore, L.; Sokol, A. A.; Catlow, C. R. A. *Surf. Sci.* **2002**, *498*, 135.
(24) Wander, A.; Harrison, N. M. *Surf. Sci.* **2003**, *529*, L281.
(25) Wang, Y.; Meyer, B.; Yin, X.; Kunat, M.; Langenberg, D.; Traeger, F.; Birkner, A.; Woll, C. *Phys. Rev. Lett.* **2005**, 95.
(26) Yan, Y.; Al-Jassim, M. M. *Phys. Rev. B* **2005**, 72.
(27) Meyer, B.; Rabaa, H.; Marx, D. *Phys. Chem. Chem. Phys.* **2006**, *8*, 1513.
(28) Ozawa, K.; Sato, T.; Oba, Y.; Edamoto, K. *J. Phys. Chem. C* **2007**, *111*, 4256.
(29) Zhou, G. C.; Sun, L. Z.; Zhong, X. L.; Chen, X. S.; Wei, L.; Wang, J. B. *Phys. Lett. A* **2007**, *368*, 112.
(30) Henrich, V. E.; Cox, P. A. *The Surface Science of Metal Oxides*; University Press: Cambridge, 1996.
(31) Ding, Y.; Wang, Z. L. *Surf. Sci.* **2007**, *601*, 425.
(32) Nosker, R. W.; Mark, P.; Levine, J. D. *Surf. Sci.* **1970**, *19*, 291.
(33) Hoffmann, R. *Rev. Mod. Phys.* **1988**, *60*, 601.
(34) Jaffe, J. E.; Hess, A. C. *Phys. Rev. B* **1993**, *48*, 7903.
(35) Ozgur, U.; Alivov, Y. I.; Liu, C.; Teke, A.; Reshchikov, M. A.; Dogan, S.; Avrutin, V.; Cho, S. J.; Morkoc, H. *J. Appl. Phys.* **2005**, 98.
(36) Becke, A. D. *J. Chem. Phys.* **1993**, *98*, 5648.
(37) Lee, C. T.; Yang, W. T.; Parr, R. G. *Phys. Rev. B* **1988**, *37*, 785.
(38) Dovesi, R.; Saunders, V. R.; Roetti, C.; Causà, M.; Harrison, N. M.; Orlando, R.; Aprà, E. *CRYSTAL03 User's Manual*;University of Torino: Torino, 2003.
(39) Corà, F.; Alfredsson, M.; Mallia, G.; Middlemiss, D. S.; Mackrodt, W.; Dovesi, R.; Orlando, R. *Structure and Bonding*; Springer Verlag: Berlin, 2004, 113.
(40) Sambrano, J. R.; Longo, V. M.; Longo, E.; Taft, C. A. *J. Mol. Struct. (theochem)* **2007**, *813*, 49.
(41) de Lazaro, S. R.; de Lucena, P. R.; Sambrano, J. R.; Pizani, P. S.; Beltran, A.; Varela, J. A.; Longo, E. *Phys. Rev. B* **2007**, 75.
(42) de Lazaro, S.; Longo, E.; Sambrano, J. R.; Beltran, A. *Surf. Sci.* **2004**, *552*, 149.
(43) Rassolov, V. A.; Pople, J. A.; Ratner, M. A.; Windus, T. L. *J. Chem. Phys.* **1998**, *109*, 1223.
(44) Ong, H. C.; Chang, R. P. H. *Appl. Phys. Lett.* **2001**, *79*, 3612.
(45) Powell, M. J. D. *Numerical Methods for Non Linear Algebraic Equations*; Gordon and Breach: London, 1970.
(46) Kokalj, A. *J. Mol. Graph.* **1999**, *17*, 176.
(47) Goano, M.; Bertazzi, F.; Penna, M.; Bellotti, E. *J. Appl. Phys.* **2007**, *102*, 083709.
(48) Decremps, F.; Datchi, F.; Saitta, A. M.; Polian, A.; Pascarelli, S.; Di Cicco, A.; Itie, J. P.; Baudelet, F. *Phys. Rev. B* **2003**, 68.
(49) Hyde, B. G.; Andersson, S. *Inorganic Crystal Structures*; Wiley: New York, 1989.
(50) Persson, P. *Chem. Phys. Lett.* **2000**, *321*, 302.
(51) Beltran, A.; Andres, J.; Calatayud, M.; Martins, J. B. L. *Chem. Phys. Lett.* **2001**, *338*, 224.
(52) Hummer, K. *Phys. Stat. Solidi B* **1973**, *56*, 249.
(53) Wander, A.; Harrison, N. M. *J. Phys. Chem. B* **2001**, *105*, 6191.
(54) Filippetti, A.; Fiorentini, V.; Cappellini, G.; Bosin, A. *Phys. Rev. B* **1999**, *59*, 8026.
(55) Wang, Y. R.; Duke, C. B. *Surf. Sci.* **1987**, *192*, 309.
(56) Mizoguchi, T.; Tatsumi, K.; Tanaka, I. *Ultramicroscopy* **2006**, *106*, 1120.
(57) Sambrano, J. R.; Nobrega, G. F.; Taft, C. A.; Andres, J.; Beltran, A. *Surf. Sci.* **2005**, *580*, 71.
(58) Vohs, J. M.; Barteau, M. A. *Surf. Sci.* **1986**, *176*, 91.

JP801718X